MATER. RES. LETT.
2018, VOL. 6, NO. 7, 365–371
https://doi.org/10.1080/21663831.2018.1461141

MATERIALS RESEARCH LETTERS
Taylor & Francis
Taylor & Francis Group

ORIGINAL REPORT

OPEN ACCESS Check for updates

Strong and ductile medium Mn steel without transformation-induced plasticity effect

B. B. He[a,b] and M. X. Huang[a,b]

[a]Department of Mechanical Engineering, The University of Hong Kong, Hong Kong, People's Republic of China; [b]Shenzhen Institute of Research and Innovation, The University of Hong Kong, Shenzhen 518000, People's Republic of China

ABSTRACT

The conventional alloy design of medium Mn steel is to optimize the transformation-induced plasticity (TRIP) effect. Here we show that a dual-phase heterogeneous structure is sufficient to develop a medium Mn steel with high yield strength ($\sim$ 1.2 GPa) and large uniform elongation ($\sim$ 14.5%). The ultra-high strength is contributed by high back-stress while the large ductility is induced by strain-gradient plasticity and back-stress hardening, both of which are inherent to dual-phase heterogeneous structure. TRIP effect is suppressed during plastic deformation. Therefore, medium Mn steel can be strong and ductile by engineering dual-phase heterogeneous structure without resorting to TRIP effect.

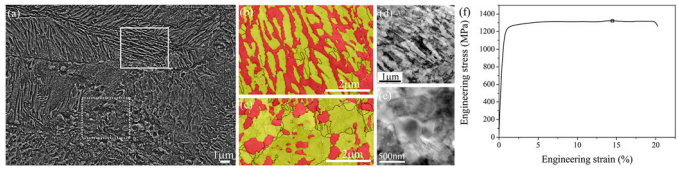

ARTICLE HISTORY
Received 1 February 2018

KEYWORDS
Medium Mn steel; phase transformation; dual-phase heterogeneous structure; defects; ultrafine-grained structure

IMPACT STATEMENT

We demonstrate that medium Mn steel can be strong and ductile by engineering dual-phase heterogeneous structure without resorting to the conventional transformation-induced plasticity (TRIP) effect.

Introduction

Advanced high-strength steels (AHSSs) are designed for structural applications in automotive industry to improve energy efficiency and reduce greenhouse gas emission [1]. Medium Mn steel is a promising candidate in the 3rd generation AHSSs due to its excellent combination of strength and ductility [2–7]. In general, medium Mn steel has a dual-phase microstructure with retained austenite grains embeded in the ferrite matrix [4,5]. The retained austenite grains may transform into martensite during plastic deformation, providing a tranformation-induced plasticity (TRIP) effect to enhance the work-hardening behavior [4,5]. It is believed that either the exhaustion of austenite grains at small strains due to their low mechanical stability or the remaining of large amount of austenite grains at large strains owing to their high mechanical stability is detrimental to the tensile properties [8]. In other words, the mechcanical stability of retained austenite grains should be optimized to achieve medium Mn steel with high strength and high ductility. Nevertheless, the formation of fresh martensite during plastic deformation will facilitate the delayed fracture induced by hydrogen embrittlement in high-strength medium Mn steels with TRIP effect [9,10]. Therefore, high-strength medium Mn steel developed by strategies that are not relying on TRIP effect will be desirable for avoiding the delayed fracture in automotive applications.

There are several strategies to develop strong and ductile metals in literatures. For instance, it is found that a bimodal grained structure can make a pure copper strong and ductile [11,12]. Recently, a unique heterogeneous lamella structure can enable ultrafine-grained titanium with coarse grained ductility [13,14]. Inspired by these pioneering studies, the present work is aimed to develop

CONTACT M. X. Huang mxhuang@hku.hk Department of Mechanical Engineering, The University of Hong Kong, Hong Kong, People's Republic of China; Shenzhen Institute of Research and Innovation, The University of Hong Kong, Shenzhen 518000, People's Republic of China

© 2018 The Author(s). Published by Informa UK Limited, trading as Taylor & Francis Group.
This is an Open Access article distributed under the terms of the Creative Commons Attribution License (http://creativecommons.org/licenses/by/4.0/), which permits unrestricted use, distribution, and reproduction in any medium, provided the original work is properly cited.

a dual-phase heterogeneous structure in a single medium Mn steel. We find that medium Mn steel can be strong and ductile by engineering dual-phase heterogeneous structure without resorting to TRIP effect.

Experiments

A medium Mn steel with a chemical composition of Fe–10%Mn–0.47%C–2%Al–0.7%V (weight percent) is employed for present study. The medium Mn steel is cast and forged into billet, followed by homogenization at 1150°C for 2.5 h to dissolve V-carbide precipitates and then hot rolled to strips with a final thickness of 4 mm. The finished hot rolling temperature is around 850°C. The hot rolled strips are warm rolled (WR) to a thickness of 2 mm at 750°C by 6 passes to refine the austenite grain size. The WR strips are then intercritically annealed (IA) at 620°C for 5 h to form granular ferrite grains and then quenched by water. This sample is termed as WR + IA sample for brevity. Large WR + IA tensile samples with a gauge length of 60 mm are fabricated from the strips along the rolling direction and are uni-axially deformed till fracture to introduce lath martensite. The small tensile samples with a gauge length of 12 mm, a width of 4 mm and a thickness of 1.9 mm are then fabricated from the gauge part of fractured large WR + IA sample. Note that the uniform elongation of large WR + IA sample is almost the same as the total elongation of 18% [15], thus the thickness of small tensile samples is homogeneous. The small tensile test samples are annealed at 700°C for 10 mins to obtain lamellar austenite grains by reverse transformation from lath martensite. Consequently, our steel with dual-phase heterogeneous structure is achieved after multiple deformation and annealing processes. The tensile tests for both large and small tensile samples are performed using a universal tensile testing machine at room temperature with a strain rate of $5 \times 10^{-4}\ s^{-1}$. The phase transformation kinetics during annealing at 700°C is investigated by Linseis dilatometer L78 in quench mode. The dilatometer sample with a length of 10 mm, a width of 4 mm and a thickness of 1.9 mm is fabricated from the gauge part of fractured large WR + IA sample. The scanning electron microscopy (SEM) observation is carried out using the Leo 1530 FEG SEM at

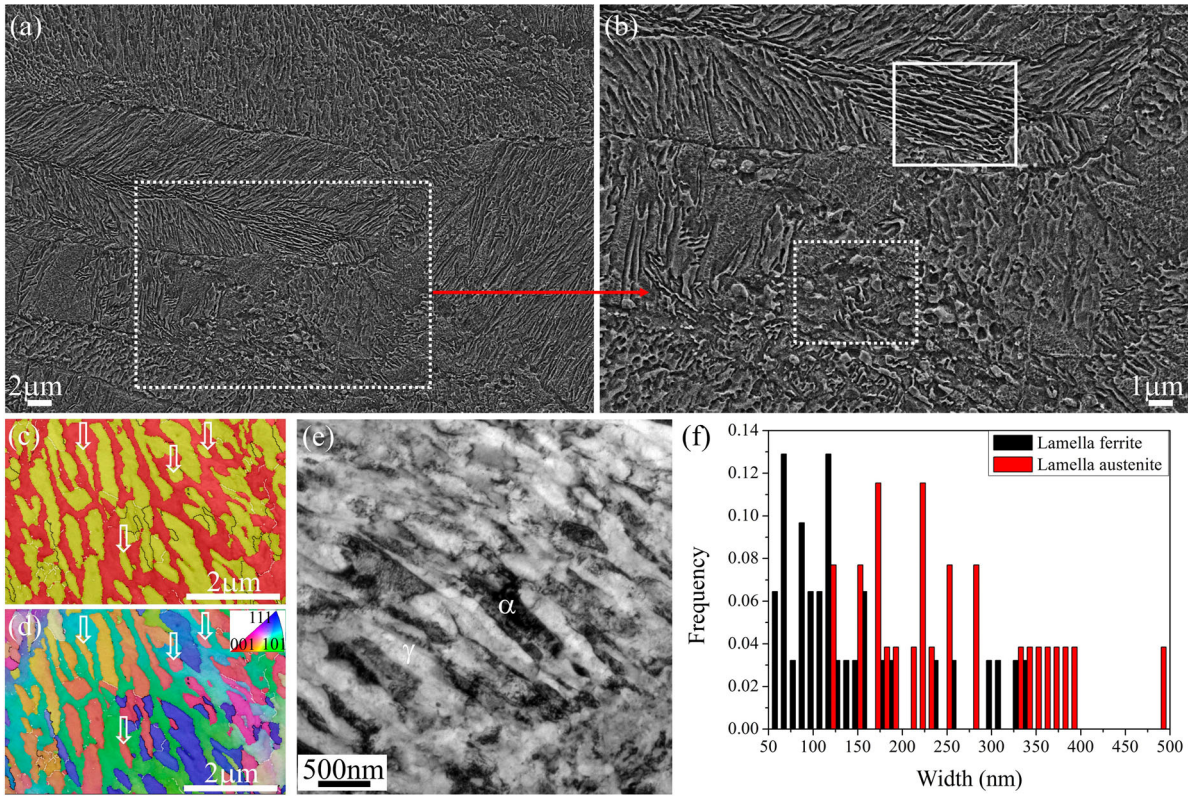

Figure 1. (a) SEM image of present medium Mn steel with dual-phase heterogeneous structure. (b) Magnified view of dashed rectangle in (a). Solid rectangle marks lamella structure; Dashed rectangle marks the granular structure. (c) EBSD phase map showing the lamella ferrite and lamella austenite. Red: ferrite; yellow: austenite. Black line represents high angle boundaries ($\theta > 15°$); white line represents low angle boundaries ($2° < \theta < 15°$). The white arrows mark austenite grains that are fully surrounded by lamella ferrite. (d) The corresponding orientation image. (e) TEM image of lamella structure—α: ferrite; γ: austenite. (f) The width distribution of lamella ferrite and lamella austenite.

5 kV. The sample for SEM observation is etched using the 2% nital solution for 60 s after conventional mechanical grinding and electro-polishing. The electro-polishing is performed in a solution of 15% perchloric acid and 85% ethanol (vol.%) at room temperature with a potential of 1 5.8 V. The transmission electron backscattered diffraction (t-EBSD) measurement is performed in Leo 1530 at 20 kV with a step size of 20 nm and the corresponding data is processed by HKL Channel 5. The transmission electron microscopy (TEM) observation is performed in a FEI Tecnai G20 at 200 kV. The element analysis is performed by using energy dispersive spectroscopy (EDS) in TEM facilities. The TEM sample is prepared by Twin-jet machine using a mixture of 5% perchloric acid and 95% ethanol (vol.%) at −30°C with a potential of 30 V. The X-ray diffraction (XRD) tests are carried out using a Cu Kα radiation for phase identification. The volume fraction of austenite is estimated based on the integrated intensities of the diffraction reflections including the (200)α, (211)α, (200)γ, (220)γ and (311)γ peaks.

Results and discussions

Our present medium Mn steel has a heterogeneous structure (Figure 1(a)), which is dominated by major lamella structure (solid rectangle in Figure 1(b)) and minor granular structure (dashed rectangle in Figure 1(b)). The lamella structure contains dual-phase microstructure of ferrite and austenite grains (Figure 1(c)). Some lamella austenite grains are fully surrounded by lamella ferrite grains (arrows in Figure 1(c,d)), suggesting that some austenite grains are nucleated at the prior martensite lath boundaries [16]. The orientation relationship between lamella austenite grains and adjacent lamella ferrite grains is close to Kurdjumov–Sachs (K–S) relation (42.85°/ < 114 >) according to the angle-axis values [17]. The lamella structure could be also confirmed by TEM observation (Figure 1(e)). Both lamella ferrite and lamella austenite have a wide spread of width distribution (Figure 1(f)). The average width of lamella ferrite and lamella austenite is estimated to be 146 and 253 nm, respectively.

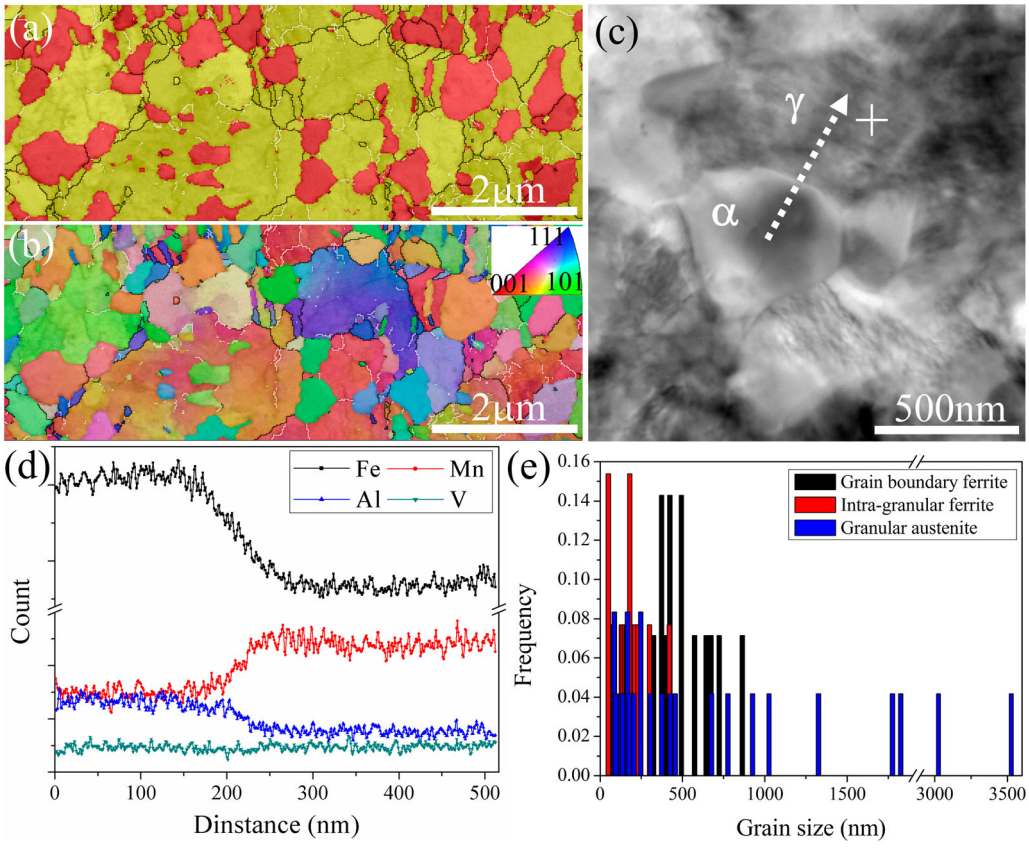

Figure 2. (a) EBSD phase map of granular structure showing the distribution of ferrite both at austenite grain boundaries and within austenite grain interior. Black line represents high angle boundaries ($\theta > 15°$); white line represents low angle boundaries ($2° < \theta < 15°$). (b) The corresponding orientation image. (c) STEM image showing granular ferrite and austenitic matrix. α: ferrite; γ: austenite. Dashed arrow marks the position of TEM-EDS line measurement. White cross marks the position of TEM-EDX spot measurement. (d) The TEM-EDS analysis showing the element partitioning between granular ferrite and austenitic matrix. (e) The grain size distribution of granular ferrite and granular austenite.

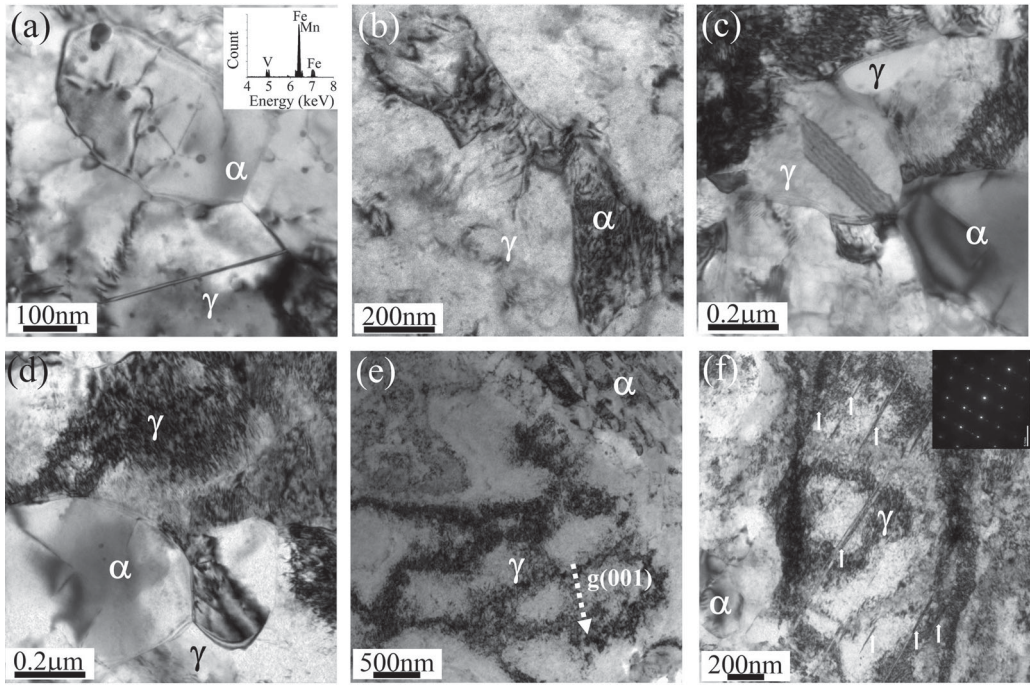

Figure 3. (a) TEM image showing the distribution of dislocations and vanadium carbide precipitates in granular ferrite. The upper inset shows the TEM-EDS spectrum of vanadium carbide precipitates. (b) TEM image showing the distribution of dislocations in lamella ferrite. (c) TEM image showing the small austenite grain. (d) TEM image of large granular austenite grain with high dislocation density. (e) TEM image of large granular austenite grain with dislocation cell structure. (f) TEM image showing the distribution of deformation nanotwins in large granular austenite grains.

In addition, the granular structure also contains a dual-phase microstructure of ferrite and austenite grains (Figure 2(a)). The ferrite grains are located either at austenite grain boundary or within austenite grain interior (Figure 2(a,b)), which could be termed as grain boundary ferrite and intra-granular ferrite, respectively. The average grain size of grain boundary ferrite and intra-granular ferrite is estimated to be 540 and 174 nm, respectively. The granular austenite grains also have different grain size. The small austenite grains are either distributed at large austenite grain boundaries or within large austenite grain interior (Figure 2(a)). These small austenite grains have different orientation with respect to the austenitic matrix (Figure 2(b)), suggesting that they could be formed by partial recrystallization of austenite during thermomechanical processing. An obvious element partitioning (Mn/Al) is observed between ferrite grain and adjacent austenite grain (Figure 2(c,d)). The Mn and Al contents in large austenite grain are found to be 11.8 and 1.9 wt.%, respectively. As compared to granular ferrite, the granular austenite has a wider spread of grain size distribution (Figure 2(e)).

The substructure of ferrite and austenite grains are revealed by TEM observation. The granular ferrite grains contain low dislocation density (Figure 3(a)). Some dislocations are tangled with the vanadium carbide precipitates (Figure 3(a)). Different from the granular ferrite, the lamella ferrite has an intensive distribution of dislocations (Figure 3(b)). The small austenite grain as marked with arrow in Figure 3(c) has a low defect density. In contrast, the large austenite grains remain in a highly deformed state with the formation of dislocation cell structure (Figure 3(d,e)), which could be due to the recovery of dislocations. Moreover, some large austenite grains also contain the deformation nanotwins (Figure 3(f)). The high thermal stability of deformation nanotwins in present medium Mn steel could be due to V-alloying as it can increase austenite recrystallization temperature [18].

The formation mechanisms of dual-phase heterogeneous structure in our steel can be revealed by investigating the specific microstructure at different deformation and annealing stages. Our steel in its hot rolled state has an almost full austenite microstructure (Figure 4(a)). The austenite grains are significantly refined during warm rolling process and partially transform to ferrite during intercritical annealing process (Figure 4(b)) [19]. A large amount of austenite grains ($\sim$56%) in WR + IA sample have transformed to martensite during plastic deformation by strain induced transformation mechanism (Figure 4(c)) [20]. The austenite reverse transformation takes place during annealing at 700°C as

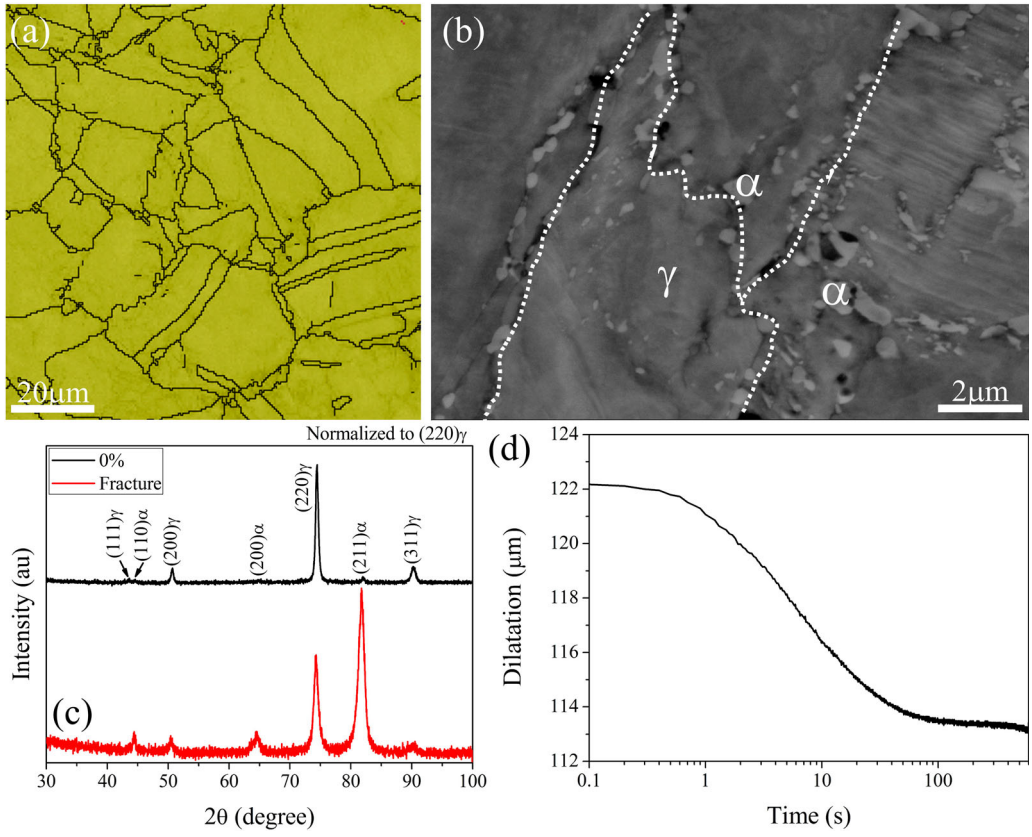

Figure 4. Evolution of microstructure in present steel during thermomechanical processing. (a) EBSD phase image of present steel in the hot rolled state. Red: martensite; yellow: austenite. (b) SEM image of WR + IA sample, showing the distribution of granular ferrite grains either at austenite grain boundaries or within austenite grain interior—α: ferrite; γ: austenite. The dashed lines represent the prior austenite grain boundaries. (c) XRD profiles of WR + IA sample prior to and after tensile test, showing the intensive formation of martensite (~ 56%) after fracture. (d) The transformation kinetics of fractured WR + IA sample during isothermal holding at 700°C for 600 s.

confirmed from the contraction of dilatometry sample (Figure 4(d)). The fast austenite reverse transformation kinetics (Figure 4(d)) could be due to intensive lath boundaries and high dislocation density in lath martensite [16]. The austenite grains tend to nucleate at and grow along the martensite lath boundaries [16], leading to the formation of lamella austenite grains (Figure 1(c)). The residual lath martensite remains in a lamella morphology with a high dislocation density (Figure 3(b)).

Our steel with dual-phase heterogeneous structure demonstrates an ultra-high yield strength of 1.2 GPa and a large uniform elongation of 14.5% (Figure 5(a,b)). The undesirable yield point phenomenon not is observed in our steel, which is consistent with the tensile behavior of other medium Mn steel with lath-like microstructure [21]. This is because the lath-like microstructure that is elongated in one direction can facilitate the dislocation accommodation and dislocation interactions, and therefore suppresses the yield point phenomenon [21]. The ultra-high yield strength of our steel can be ascribed to the high back-stress developed in present dual-phase heterogeneous structure. Upon tensile testing, the heterogeneous yielding takes place in our heterogeneous structure because it consists of soft and hard phases owing to their different size and sub-structures (Figures 1–3). This heterogeneous yielding induces a long-range back-stress which can increase the flow stress of soft phase and consequently leads to an ultra-high yield strength of our steel [13].

Different from the intensive martensitic transformation in the WR + IA sample (Figure 4(b,c)), the martensitic transformation in our steel with dual-phase heterogeneous structure is largely suppressed during plastic deformation (Figure 5(c)). In other words, the retained austenite grains have high mechanical stability. This could be due to austenite grain refinement [22–24], C/Mn enrichment [25] and high defect density [26]. The lamella austenite grains have an average grain size of 253 nm (Figure 1(f) and could have high C/Mn contents due to the nucleation of austenite at carbides in martensite lath boundaries [27]. The granular austenite grains have a wide spread of grain size distribution (Figure 2(e)).

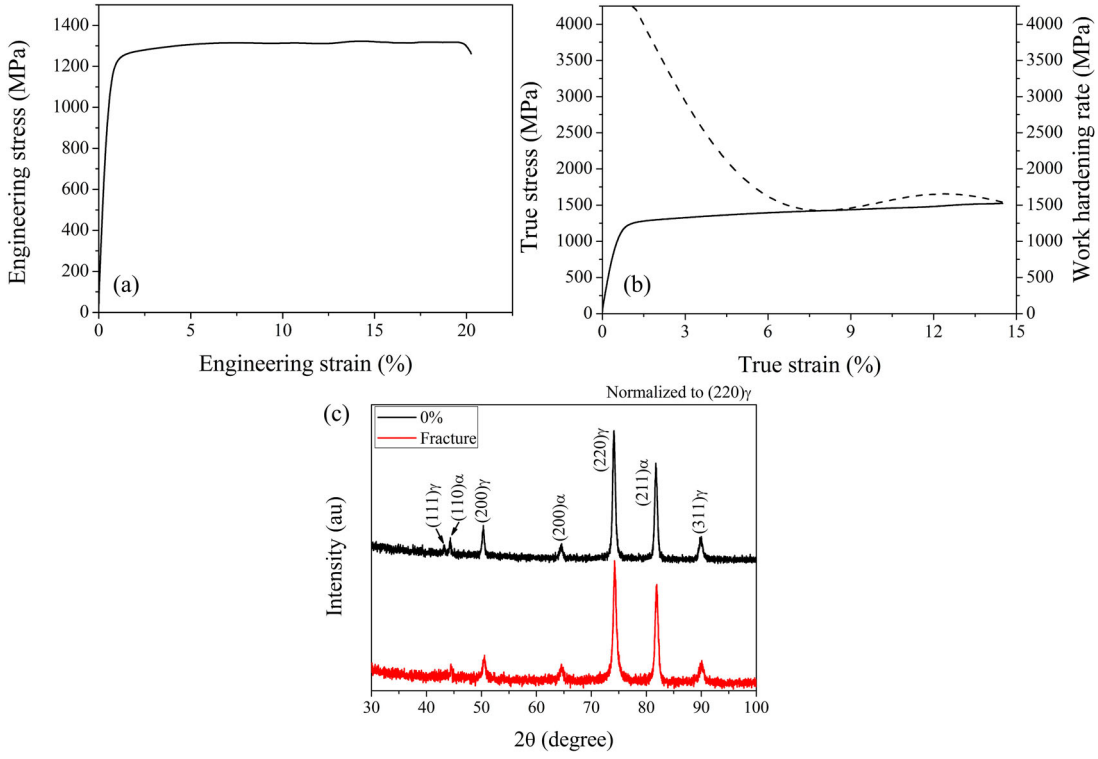

Figure 5. (a) Engineering stress strain curves of our steel with dual-phase heterogeneous structure. Hollow square marks the ultimate tensile strength. (b) The corresponding true stress–strain curve and work-hardening curve. (c) XRD profiles of our steel with dual-phase heterogeneous structure prior to and after tensile test, showing a negligible decrease of austenite volume fraction from 57% down to 55% after fracture. The decreased amount (~ 2%) of austenite volume fraction is within the error of XRD measurement (~ 5%).

The large granular austenite grains tend to be less stable as compared to the tiny austenite grains [22–24]. However, these large granular austenite grains could also have high mechanical stability due to their high defect density (Figure 3(d–f)) [26] and high Mn content (Figure 2(d)) [25].

Despite of suppressed TRIP effect, our steel with dual-phase heterogeneous structure can still have a moderate work-hardening rate across a large uniform elongation (~ 14.5%) as shown in Figure 5(b). Note that the amount of deformation nanotwins are not obviously increased in the fractured sample as revealed by TEM observation. Therefore, the twinning-induced plasticity effect is not important here. Our steel has a dual-phase heterogeneous structure with lamella structure and granular structure (Figures 1,2). Each structure has a dual-phase microstructure with a wide grain size distribution (Figures 1(f) and 2(e)). Moreover, the constituting phases have different sub-structures (Figure 3), indicating their different mechanical properties. For a material like the present steel with microstructural and mechanical inhomogeneity, the corresponding uni-axial tensile deformation shall generate a large strain gradient among grains and phases, which is accommodated by an excessively large number of geometrically necessarily dislocations (GNDs) piling-up at the grain and phase boundaries [28] and therefore results in enhanced work-hardening behavior as predicted by the strain-gradient plasticity theory (Figure 5(b)) [29]. Moreover, the generation of intensive GNDs will also develop large long-range back-stress at the boundaries, which will improve the strain hardening behavior [13]. The operation of back-stress hardening could even lead to an upturn in work-hardening curve of our steel (Figure 5(b)), which has been also observed in pure Ti with heterogeneous lamella structure [13]. Therefore, the large ductility of our steel with dual-phase heterogeneous structure is mainly contributed by the strain-gradient plasticity and back-stress hardening.

Conclusions

In summary, a strong and ductile medium Mn steel with a dual-phase heterogeneous structure is developed by multiple deformation and annealing processes. This dual-phase heterogeneous structure contains major lamella structure and minor granular structure. Both of these two structures have a dual-phase microstructure of ferrite and austenite grains. The formation mechanism of this dual-phase heterogeneous structure is revealed by detailed

microstructural characterization at varied thermomechanical processing stages. The TRIP effect is largely suppressed in present medium Mn steel with dual-phase heterogeneous structure due to austenite grain refinement, C/Mn enrichment and high defect density. Nevertheless, this steel can still be ductile, which is ascribed to the strain-gradient plasticity and back-stress hardening.

Disclosure statement

No potential conflict of interest is reported by the authors.

Funding

M. X. Huang acknowledges the financial support from National Natural Science Foundation of China [grant number U1764252, U1560204] and Research Grants Council of Hong Kong [grant number 17255016, 17203014, C7025-16G].

References

[1] He BB, Hu B, Yen HW, et al. High dislocation density-induced large ductility in deformed and partitioned steels. Science. 2017;357:1029–1032.
[2] Suh DW, Kim SJ. Medium Mn transformation-induced plasticity steels: recent progress and challenges. Scripta Mater. 2017;126:63–67.
[3] He BB, Luo HW, Huang MX. Experimental investigation on a novel medium Mn steel combining transformation-induced plasticity and twinning-induced plasticity effects. Int J Plast. 2016;78:173–186.
[4] Shi J, Sun XJ, Wang MQ, et al. Enhanced work-hardening behavior and mechanical properties in ultrafine-grained steels with large-fractioned metastable austenite. Scripta Mater. 2010;63:815–818.
[5] Cai ZH, Ding H, Misra RDK, et al. Austenite stability and deformation behavior in a cold-rolled transformation-induced plasticity steel with medium manganese content. Acta Mater. 2015;84:229–236.
[6] Gibbs PJ, De Cooman B, Brown DW, et al. Strain partitioning in ultra-fine grained medium-manganese transformation induced plasticity steel. Mater Sci Eng A. 2014;609:323–333.
[7] Moor E D, Matlock DK, Speer JG, et al. Austenite stabilization through manganese enrichment. Scripta Mater. 2011;64:185–188.
[8] Ryu JH, Kim DI, Kim HS, et al. Strain partitioning and mechanical stability of retained austenite. Scripta Mater. 2010;63:297–299.
[9] McCoy R, Gerberich W. Hydrogen embrittlement studies of a TRIP steel. Metall Trans. 1973;4:539–547.
[10] Zhu X, Li W, Zhao H, et al. Hydrogen trapping sites and hydrogen-induced cracking in high strength quenching & partitioning (Q&P) treated steel. Int J Hydrogen Energy. 2014;39:13031–13040.
[11] Wang Y, Chen M, Zhou F, et al. High tensile ductility in a nanostructured metal. Nature. 2002;419:912–915.
[12] Ma E, Zhu T. Towards strength–ductility synergy through the design of heterogeneous nanostructures in metals. Mater Today. 2017;20:323–331.
[13] Wu XL, Yang MX, Yuan FP, et al. Heterogeneous lamella structure unites ultrafine-grain strength with coarse-grain ductility. Proc Nat Acad Sci USA. 2015;112:14501–14505.
[14] Wu XL, Zhu YT. Heterogeneous materials: a new class of materials with unprecedented mechanical properties. Mater Res Lett. 2017;5:527–532.
[15] Hu B, Luo H, Yang F, et al. Recent progress in medium-Mn steels made with new designing strategies, a review. J Mech Sci Technol. 2017;33:1457–1464.
[16] Nakada N, Mizutani K, Tsuchiyama T, et al. Difference in transformation behavior between ferrite and austenite formations in medium manganese steel. Acta Mater. 2014;65:251–258.
[17] Sato H, Zaefferer S. A study on the formation mechanisms of butterfly-type martensite in Fe–30% Ni alloy using EBSD-based orientation microscopy. Acta Mater. 2009;57:1931–1937.
[18] Scott C, Remy B, Collet J-L, et al. Precipitation strengthening in high manganese austenitic TWIP steels. Int J Mater Res. 2011;102:538–549.
[19] Dong H, Sun X. Deformation induced ferrite transformation in low carbon steels. Curr Opin Solid State Mater Sci. 2005;9:269–276.
[20] Olson G, Cohen M. Kinetics of strain-induced martensitic nucleation. Metall Trans A. 1975;6:791–795.
[21] Steineder K, Krizan D, Schneider R, et al. On the microstructural characteristics influencing the yielding behavior of ultra-fine grained medium-Mn steels. Acta Mater. 2017;139:39–50.
[22] Jimenez-Melero E, van Dijk NH, Zhao L, et al. Characterization of individual retained austenite grains and their stability in low-alloyed TRIP steels. Acta Mater. 2007;55:6713–6723.
[23] Yang HS, Bhadeshia HKDH. Austenite grain size and the martensite-start temperature. Scripta Mater. 2009;60:493–495.
[24] Zhang S, Findley K. Quantitative assessment of the effects of microstructure on the stability of retained austenite in TRIP steels. Acta Mater. 2013;61:1895–1903.
[25] Lee S, Lee SJ, De Cooman BC. Austenite stability of ultrafine-grained transformation-induced plasticity steel with Mn partitioning. Scripta Mater. 2011;65:225–228.
[26] Chatterjee S, Wang HS, Yang JR, et al. Mechanical stabilisation of austenite. Mater Sci Technol. 2006;22:641–644.
[27] Lee S, De Cooman BC. Influence of carbide precipitation and dissolution on the microstructure of ultra-fine-grained intercritically annealed medium manganese steel. Metall Mater Trans A. 2016;47:3263–3270.
[28] Ashby MF. The deformation of plastically non-homogeneous materials. Philos Mag. 1970;21:399–424.
[29] Gao HJ, Huang YG, Nix WD, et al. Mechanism-based strain gradient plasticity? I. Theory. J Mech Phys Solids. 1999;47:1239–1263.